High-energy electron-energy-loss study of sodium-tungsten bronzes

M. Kielwein,* K. Saiki,† and G. Roth
Forschungszentrum Karlsruhe, Institut für Nukleare Festkörperphysik, Postfach 3640, D-76021 Karlsruhe, Federal Republic of Germany

J. Fink and G. Paasch
Institut für Festkörper- und Werkstofforschung Dresden e.V., Institut für Festkörperforschung, Postfach 270016, D-01171 Dresden, Federal Republic of Germany

R. G. Egdell
University of Oxford, Inorganic Chemistry Laboratory, South Parks Road, Oxford OX1 3QR, United Kingdom
(Received 21 November 1994)

Single-crystal metallic cubic sodium-tungsten bronzes Na_xWO_3 ($x \geq 0.25$) and $Na_xTa_yW_{1-y}O_3$ ($x-y=0.42$) and monoclinic reduced $WO_{3-\delta}$ have been investigated by high-energy electron-energy-loss spectroscopy (EELS) in transmission. For all electron densities the volume plasmon dispersion appears to be positive quadratic in momentum transfer q. The dispersion coefficient is much smaller than that predicted from the random-phase approximation for one isotropic parabolic band. This deviation can be reduced by recognizing the threefold degeneracy of the conduction-band t_{2g} states in an octahedral field and narrowing of these bands with increasing sodium content. Anisotropy of the dispersion between the (100) and (110) direction is not observed. Optical effective masses $m^*(x)$ of the conduction electrons and background dielectric constants $\epsilon_\infty(x)$ have been determined and compare well with data from optical spectroscopy and EELS in reflection, but not with photoemission results. This discrepancy is a result of the photoemission-data evaluation in which the conduction-band degeneracy was neglected. Na $2p$ core-level excitation energies argue against an admixture of sodium orbitals to the conduction band near the metal-nonmetal transition at $x \sim 0.2$. Na $3s$ states admixed to O $2p$ states are observed at about 10–11 eV above the Fermi level in O $1s$ absorption edges. The x dependence of m^* and of the width of the O $1s$ absorption edge of Na_xWO_3 supports a model of conduction-band narrowing with increasing Na concentration.

I. INTRODUCTION

The sodium-tungsten bronzes Na_xWO_3 ($0 \leq x \leq 1$) can be considered as solid solutions of metal atoms (Na) in a transition-metal oxide (WO_3) sublattice.[1] Their structural and electronic properties have been investigated very extensively by means of x-ray diffraction,[2] neutron diffraction,[3,4] inelastic neutron scattering,[5] nuclear magnetic resonance (NMR),[6–9] photoemission (PES),[10–16] inverse PES,[17] electron-energy-loss spectroscopy (EELS) in reflection,[14,18–21] optical,[22–25] specific heat,[26,27] magnetic susceptibility,[27,28] and chemical potential[29] measurements. At room temperature a slightly distorted cubic perovskite structure is thermodynamically stable for $x > 0.4$, but the cubic phase can be synthesized under nonequilibrium conditions down to $x \sim 0.2$.[30] By varying the composition, the conduction electron concentration can be varied over a wide range within the cubic phase regime. A metal-nonmetal transition occurs at approximately $x \sim 0.2$.[15,31,32]

The electronic structure is qualitatively understood in terms of a band model proposed by Goodenough.[33] The valence band and the conduction band are composed of oxygen $2p$ and tungsten $5d$ orbitals, respectively. The five W $5d$ orbitals are split by the crystal field into two σ-type e_g and three lower lying π-type t_{2g} bands. The latter interact with the O $2p\pi$ orbitals and form the antibonding t_{2g} conduction band, which upon doping with Na accepts the Na $3s$ electrons. The conduction-band states are threefold degenerate at the Γ point, and the threefold degeneracy is retained along Γ-R.[34,35] However, along the Γ-X direction the degeneracy is lifted and one of the t_{2g} bands remains flat. Korringa-Kohn-Rostoker[34] (KKR) and linear combination of atomic orbitals[35] (LCAO) band-structure calculations for $x=1$ are very similar to that of idealized cubic WO_3 (Refs. 34 and 35) and ReO_3 (Ref. 36) within the conduction-band region: the sodium orbitals lie well above the Fermi level and do not contribute to the conduction band. This idea is supported by the fact that the conductivity in M_xWO_3 (M=Na, Li) is only dependent on x and not on the alkali metal M (Ref. 37), and that there is no Knight shift (at high x) in ^{23}Na NMR (Ref. 9).

From the band-structure calculations[34,35] for $x=1$ and idealized cubic WO_3 it has been deduced that the sodium-tungsten bronzes exhibit rigid-band behavior in the region of the valence and conduction band. The validity of the rigid-band model has been discussed in relation to photoemission data for several years.[11,12,38,39] High-resolution PES and high-resolution EELS in reflection (HREELS) measurements by Egdell and Hill[13,14,20] on cubic polycrystalline Na_xWO_3 ($x \geq 0.26$) led to the conclusion that the conduction band narrows with increasing x in agreement with ideas put forward by

Goodenough[33] many years earlier. Using a free-electron description this narrowing can be transformed into a dependence of the effective mass on the sodium content which, however, does not prove the correctness of the free-electron description. Actually, regardless of the x-dependent bandwidth the band-structure calculations[34,35] show the existence of three partially filled bands with an x-independent topology of the three Fermi surfaces. From the band structure[34–36] one can deduce their shape: one Fermi surface is nearly spherical, the second is a warped sphere, and the third consists of three orthogonal and cross-linked cylinders. A semiempirical LCAO model[40,41] based on W $5d$ and O $2p$ orbitals simplifies this band structure to three independent two-dimensional bands, i.e., three cylinders as Fermi surfaces. With only two x-dependent parameters this model describes well the electronic specific heat, the magnetic susceptibility, and approximately the (optical) effective mass. Although this model overestimates two dimensionality even the apparently free-electron-like high-resolution PES data[14] are described quite reasonably when the experimental resolution is taken into account. The two-dimensional character of the Fermi surface is supported also by inelastic neutron scattering measurements[5] which reveal a large Kohn anomaly in the acoustic phonon dispersion and by positron annihilation experiments.[42]

In $Na_xTa_yW_{1-y}O_3$ tantalum compensates the conduction electron density which is then determined by x-y.[1,43,44] These compositions are of interest as they allow direct growth of cubic crystals with lower carrier densities than is possible in the uncompensated bronzes.

In the present paper, we report on investigations of the electronic structure of the system Na_xWO_3 by EELS in transmission. The loss function and core-level excitations have been measured for $0.25 \leq x \leq 0.68$. Furthermore, the dispersion of the charge carrier plasmon as a function of momentum transfer has been determined. To our knowledge, this is the first systematic study of the dispersion of a charge carrier plasmon in a degenerately doped oxide where the carrier concentration can be varied over a wide range. Strong deviations of dispersion parameters from free-electron random-phase approximation (RPA) values are observed which partly can be explained by band-structure effects.

II. THEORETICAL BACKGROUND

The general volume plasmon dispersion relation for an electron subsystem with density n is[45]

$$\omega(q)=\omega_P+Aq^2+O(q^4) , \tag{1a}$$

$$\omega_P^2=\frac{4\pi ne^2}{\epsilon_\infty m_{\text{opt}}} , \tag{1b}$$

where the plasmon frequency ω_P contains the optical effective mass m_{opt} and the background dielectric constant ϵ_∞. For a free-electron gas with effective mass m^* ($=m_{\text{opt}}$) the dispersion coefficient A is conveniently expressed via the dimensionless dispersion coefficient α as

$$A=\frac{\hbar}{m^*}\alpha . \tag{2a}$$

In the RPA for a free-electron system the dimensionless dispersion coefficient α_{RPA} is given by

$$\alpha_{\text{RPA}}=\frac{3}{5}\frac{E_F}{\hbar\omega_P} , \tag{2b}$$

where $E_F=(\hbar k_F)^2/(2m^*)$ is the Fermi energy and k_F is the Fermi wave vector. In a free-electron system within the RPA strong damping occurs above a critical wave vector $q_c \sim [\hbar\omega_P/(2E_F)]k_F$ due to decay of the plasmon into electron-hole pairs. In a real solid the whole plasmon usually lies in the continuum of interband transitions giving rise to damping[46] and hence to the finite width of the loss function. For simple metals a quadratic dependence of the linewidth $\Delta E_{1/2}(q)=\Delta E_{1/2}(0)+Bq^2$ for low momentum transfer q is then expected.[47]

RPA accounts correctly for the long-range Coulomb interaction and therefore is exact in the long-wavelength ($q\rightarrow 0$)–high-density limit. The latter corresponds to $r_s \ll 1$, r_s being the density parameter which for the free-electron gas is determined by $r_s a_0=(4\pi n/3)^{-1/3}$, with the Bohr radius $a_0=\hbar^2/(me^2)$ where m is the free-electron mass. Whereas the RPA accounts well for many properties of nearly free electron (NFE) metals ($2<r_s<6$), the plasmon dispersion coefficient is significantly reduced with decreasing density by local field corrections which account for short-range exchange and correlation effects. The dimensionless dispersion coefficient is then given by

$$\alpha=\alpha_{\text{RPA}}\left[1-\tfrac{5}{12}\gamma(r_s)\left[\frac{\hbar\omega_P}{E_F}\right]^2\right] , \tag{3}$$

where γ is the $(q/k_F)^2$ coefficient of the low q expansion of the local field correction function in the static limit $G(q,\omega\rightarrow 0)$.[48]

Since Na_xWO_3 is a solid solution of sodium in tungsten oxide the conduction electron density is rather small, i.e., by using the free-electron expression the density parameter is even larger ($r_s \sim 5$–7) than in the alkali metals, suggesting apparently the need to consider local field corrections according to Eq. (3). Actually, these conduction electrons form a subsystem where band-structure effects lead to an effective mass $m^* < m$ and the polarizability of all other electrons results in a screening of the Coulomb interaction by the background dielectric constant as e^2/ϵ_∞. Thus the density parameter is reduced to an effective value $r_s^*=r_s[m^*/(m\epsilon_\infty)]$. In our case r_s^* lies in the range of 0.5 to 0.7 as shown below and one has to expect the RPA to be better justified than in any elemental NFE metal. In this case the observed deviation of the plasmon dispersion from its free-electron RPA value has to be attributed to the deviation from free-electron behavior due to details of the band structure.

We consider band-structure effects within the Ehrenreich-Cohen (EC) formula[49] for the dielectric function although crystal local field effects[50] could also be important due to the localized character of the wave functions forming the conduction band. In the past band-structure effects on the plasmon dispersion have been

considered either within a pseudopotential perturbation scheme[51] or by full band structure based evaluation of the loss function using the EC formula.[52] But to our knowledge the following important peculiarity has not been mentioned explicitly until now. The usual form (2) for the free-electron dispersion coefficient does not reflect those dependences needed to understand what happens when there are several conduction bands instead of only one. The derivation discussed below in more detail shows that the transition to several bands is possible after reformulating Eqs. (2a) and (2b) by using Eq. (1b) as

$$A=\frac{3}{5}\frac{4\pi e^2}{\epsilon_\infty m^{*2}}\frac{nE_F}{\omega_P^3}\rightarrow\frac{3}{5}\frac{4\pi e^2}{\epsilon_\infty m^{*2}\omega_P^3}\sum_{i=1}^{M} n_i E_{F,i}\ , \quad (4)$$

where in the second step we assumed for simplicity the existence of M identical parabolic bands with the density $n_i=n/M$. Compared to the one-band system with $E_F\sim n^{2/3}$ the M bands have all the same Fermi energy $E_{F,i}\sim n_i^{2/3}=(1/M)^{2/3}n^{2/3}$ giving $(1/M)^{2/3}E_F$. Then the sum in Eq. (4) yields $\sum_{n_i}E_{F,i}=M(n/M)(1/M)^{2/3}E_F$ and consequently the dispersion coefficient A is reduced by the factor $(1/M)^{2/3}$ compared to the one-band case. Thus, in the case $M=3$ the dispersion coefficient would be smaller by a factor of 0.48 compared to a naive application of Eqs. (2a) and (2b). A more general formulation for the plasmon dispersion used below is given in the Appendix. Regarding the critical wave vector q_c within this three-NFE-band model, whereas the plasmon frequency ω_P remains unchanged compared to the one-band case, we obtain an increased critical wave vector $q_c^*=3^{1/3}q_c\sim 1.44q_c$ due to the dependence of q_c on k_F.

III. EXPERIMENT

Large cubic single crystals of the higher doped bronzes Na_xWO_3 ($x=0.57$ and 0.68) were prepared by electrolytic reduction of a molten mixture of tungsten oxide WO_3 and sodium tungstate Na_2WO_4. A cubic single crystal with $x=0.25$ was prepared by surrounding an $x=0.57$ single crystal with WO_3 powder and out-diffusing some sodium. This blue sample showed small visible red-colored inclusions with higher sodium concentration which could easily be cleaved off. A blue-colored cubic single crystal of a tantalum-substituted tungsten bronze $Na_xTa_yW_{1-y}O_3$ ($x=0.62$, $y=0.20$) was grown by electrolytic reduction of a melt consisting of Na_2WO_4, WO_3, and Ta_2O_5.

The accurate determination of the sodium and tantalum concentration in the tungsten bronzes is very important because from this the conduction electron density and thus the free electron plasmon frequency is calculated. The sodium concentration x of the uncompensated bronzes were determined applying the well-established Vegard relationship for the lattice constants $a(x,y=0)$ (see Ref. 2):

$$a(x,y=0)=3.7845+0.0821x\ \ (\text{Å})\ . \quad (5)$$

The lattice parameters were measured with an accuracy of 10^{-4} Å by x-ray diffraction (see Table I) on powdered material from the single crystals using a STOE diffractometer with a position sensitive detector and Cu $K\alpha$ radiation. For calibration silicon was used as a stan-

TABLE I. Data of the sodium-tungsten bronzes: x-ray lattice parameters a; Na (x) and Ta (y) content, determined via Eqs. (5) and (6), respectively; conduction electron density $n=(x-y)/a^3$; and the density parameter $r_s^*=(m^*/\epsilon_\infty)r_s$, with effective mass m^* and background dielectric constant ϵ_∞. Fit parameters for the dispersion of the volume plasmon $\hbar\omega(q)=\hbar\omega_P+\hbar Aq^2$ with $\hbar A=(\hbar^2/m^*)\alpha$, the RPA dispersion coefficient α_{RPA} from Eq. (2b), and fit parameters for the dispersion of the plasmon linewidth $\Delta E_{1/2}(q)=\Delta E_{1/2}(0)+Bq^2$. Critical wave vectors (assuming three NFE bands) $q_c^*=3^{1/3}q_c$.

a (Å)	x	y	n (10^{22} cm^3)	ϵ_∞
3.8050(1)	0.25		0.45	6.15
3.8470(1)	0.62	0.20	0.74	6.10
3.8311(1)	0.57		1.01	5.30
3.8404(1)	0.68		1.20	5.20

m^*/m	r_s	r_s^*	$\hbar\omega_P$ (eV)	$\hbar A$ (eV Å^2)
0.44	7.08	0.51	1.52(3)	4.8(10)
0.66	6.02	0.65	1.59(1)	4.68(20)
0.66	5.42	0.68	1.99(1)	2.39(4)
0.72	5.12	0.71	2.11(1)	2.07(17)

α	α_{RPA}	$\Delta E_{1/2}(0)$ (eV)	B (eV Å^2)	q_c^* (Å^{-1})
0.28(6)	0.89	0.64	1.70(37)	0.25
0.41(3)	0.79	0.71	2.98(34)	0.33
0.21(1)	0.78	0.33	1.44(4)	0.37
0.20(2)	0.76	0.35	1.14(6)	0.40

TABLE II. A comparison of the x-ray lattice parameters a_{exp} (Ref. 44) of Ta-compensated sodium-tungsten bronzes $Na_xTa_yW_{1-y}WO_3$ with those calculated (a_{cal}) via Eq. (6), which is a linear fit to $a_{exp}(x,y)$.

x	y	a_{exp} (Å)	a_{cal} (Å)
0.64	0.25	3.854	3.852
0.60	0.13	3.840	3.841
0.33	0.11	3.816	3.815
0.29	0.23	3.816	3.816
0.28	0.13	3.811	3.812

dard.

To determine the sodium and tantalum concentration of the Ta-compensated bronze a relation similar to Eq. (5) was deduced from data on five $Na_xTa_yW_{1-y}O_3$ crystals published by Doumerc *et al.*[44] Assuming a linear Vegard dependence also on y within the cubic phase regime this yields

$$a(x,y)=3.7845+0.0821x+[0.0087+0.0807x]y \quad (\text{Å}) . \tag{6}$$

The excellent agreement of the x-ray lattice constants with those calculated from Eq. (6) is shown in Table II. For the Ta-containing crystal examined in this work a lattice constant of 3.8470 Å was determined from x-ray diffraction and a refinement of the measured Bragg intensities for a Ta-free structure gave a sodium occupancy $x=0.62$. From Eq. (6) it then follows that $y=0.20$.

Thin films of about 1000 Å thickness were cut in air from the crystals by an ultramicrotome using a diamond knife. Films with an area of approximately (0.6×0.6) mm^2, which sometimes had a slight wavy structure due to the cutting procedure, were picked up from the cutting edge by a one-hair brush and fixed in standard electron microscope Cu folding grids.

The orientation and quality of the films were controlled in the spectrometer by elastic electron scattering. In most cases the momentum transfer was chosen to be in the (100) direction.

All the spectra were taken at room temperature under UHV conditions using a 170-keV transmission EELS spectrometer described elsewhere.[53] For valence-band excitations, Na $2p$ core-level excitations, and elastic electron scattering the energy and momentum transfer resolution were chosen to be 160 meV and 0.06 Å^{-1}, respectively. O $1s$ absorption edges were measured with an energy and momentum transfer resolution of 440 meV and 0.12 Å^{-1}, respectively.

IV. RESULTS

A. Excitations at small momentum transfer

Qualitatively, the measured loss spectra of the Na_xWO_3 films are quite similar for different x. This is also valid for the Ta-substituted sample. We therefore show in this section only the results for the $x=0.68$ crystal which are representative for the others.

After correcting the loss spectrum, measured in an energy region of 0.3 to 75 eV at $q=0.1$ Å^{-1}, for finite momentum transfer resolution[54,55] and multiple scattering contributions[55,56] the contribution of the direct beam centered at zero energy loss has been removed. Furthermore, contributions from surface plasmons appearing at the low-energy side (see Sec. IV B) of the volume plasmon (VP) excitation (see Fig. 1), have been removed by fitting a Drude-like function on this side of the VP applying extrapolated data for the full width at half maximum (FWHM) and the peak intensity of the VP from higher momentum transfer to $q=0.1$ Å^{-1}. Since the surface plasmon decreases with q^{-3} (Ref. 55) while the VP decreases with q^{-2} this extrapolation is feasible. The use of a Drude model to correct the low-energy data is reasonable because optical ellipsometry measurements of the dielectric function of Na_xWO_3 ($x>0.5$) show a Drude-like behavior for $\hbar\omega<2.3$ eV.[25]

Then a Kramers-Kronig analysis was performed in order to obtain the absolute value of the loss function

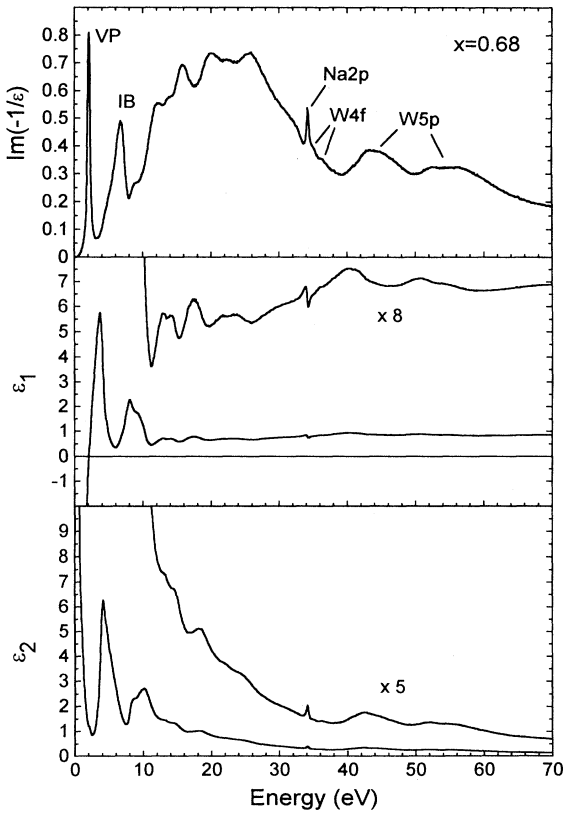

FIG. 1. The loss function Im $(-1/\epsilon)$, real part ϵ_1, and imaginary part ϵ_2 of the dielectric function of $Na_{0.68}WO_3$ for momentum transfer $q=0.1$ Å^{-1}. VP indicates the volume plasmon excitation. The peak IB corresponds to an interband transition lying at 4.1 eV in ϵ_2. Tungsten and sodium core-level excitations are denoted by Na $2p$, W $4f$, and W $5p$.

$\mathrm{Im}(-1/\epsilon)$ and to determine the dielectric function $\epsilon=\epsilon_1+i\epsilon_2$. Figure 1 shows the resulting loss function $\mathrm{Im}(-1/\epsilon)$ of $Na_{0.68}WO_3$ for $q=0.1$ Å^{-1}. The scale of the loss function was derived from the condition $\mathrm{Re}[1/\epsilon(\omega\rightarrow 0)]=0$ for a metallic material. At 2.1 eV a very sharp VP peak appears which is caused by the collective excitation of the conduction-band electrons.[18] Interband transitions (IB's) from the valence band to the conduction band cause a maximum in the loss function at 6.8 eV.[18,41]

There are several structures between 8 and 26 eV which have maxima at 9, 12.2, 13.7, 15.6, 20, 22.5, and 25.6 eV. At ~32 eV a weak broad shoulder is observed below the onset of the Na $2p$ core-level excitation. These peaks are probably due to further interband transitions and screened valence-band plasmons of the σ and π electrons.[19]

For $x=0.57$ and 0.68 and the Ta-compensated sample the Na $2p$ core-level excitation (see Fig. 2) appears with a maximum at $\hbar\omega=(34.24\pm0.02)$ eV. In metallic sodium this peak lies at 30.9 eV,[57] the shift of 3.3 eV being due to the oxidation of the Na atom in the tungsten bronzes. For $x=0.25$ the Na $2p$ core-level excitation is shifted to (34.48 ± 0.02) eV. This 0.24-eV shift to higher energy in the $x=0.25$ sample also appears for all other high-energy excitations ($\hbar\omega\geq 5$ eV) in the loss spectrum. The intensities of the Na $2p$ excitations are proportional to the sodium content x.

The W $4f_{7/2}$ and W $4f_{5/2}$ core-level excitations appear with broad maxima at approximately $\hbar\omega\sim 34.7$ eV and ~36.5 eV, respectively.[19] The separation is due to a spin-orbit splitting of 2.20 eV.[58] The rather broad W $5p_{3/2}$ and W $5p_{1/2}$ core-level structures have broad maxima at $\hbar\omega\sim 43$ eV and ~52 eV, respectively.[19] The energy difference corresponds to a spin-orbit splitting of 8.5 eV.

In Fig. 1 we also show the real part ϵ_1 and the imaginary part ϵ_2 of the dielectric function of $Na_{0.68}WO_3$. The energy of the lowest interband transition is at 4.10 eV as can be seen from the ϵ_2 curve. For $x=0.57$ and the Ta-compensated sample $(x-y=0.42)$ this peak lies at the same energy, while for $x=0.25$ it appears at 3.85 eV.

Following Dietz *et al.*[18] a background dielectric constant ϵ_∞ can be deduced from the Drude model where ϵ_1 is given by

$$\epsilon_1(\omega)=\epsilon_\infty-\frac{\Omega_P^2}{m^*}\frac{1}{\omega^2+\Gamma^2}\ . \tag{7}$$

Here, Ω_P is the free-electron plasmon frequency. A plot of ϵ_1 versus $1/(\omega^2+\Gamma^2)$ for $\hbar\omega<2.3$ eV yields the extrapolated interception $\epsilon_\infty=5.20$ with the ϵ_1 axis (see Fig. 3). For the FWHM $\hbar\Gamma$ of the volume plasmon we used the value at $q\sim 0.2$ Å^{-1} where contributions from the surface plasmon excitation are almost negligible (see Sec. IV B).

In Fig. 4 we show ϵ_∞ values derived from the present ϵ_1 values according to Eq. (7) together with results derived from optical measurements on Na_xWO_3 $(x\geq 0.5)$ (Ref. 25), WO_3 (Refs. 25 and 59), and the related compound ReO_3 (Ref. 60). The present values for ϵ_∞ are also listed in Table I.

The optical effective mass m^* of the conduction-band electrons can then be calculated via

$$m^*\epsilon_\infty=\left[\frac{\Omega_P}{\omega_P(q=0)}\right]^2\ . \tag{8}$$

The plasma frequency $\omega_P(q=0)$ is obtained from an extrapolation of momentum-dependent data to $q=0$. For $x=0.68$ we obtain a value of $\hbar\omega_P=2.11$ eV leading to $m^*=0.72$. A plot of m^* versus sodium concentration x is shown in Fig. 5 (see also Table I). Our data compare

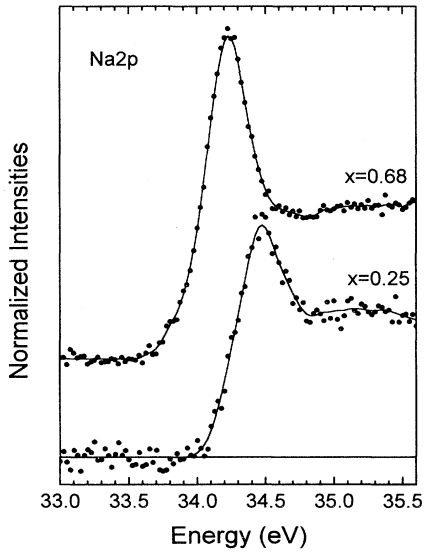

FIG. 2. The Na $2p$ core-level excitation of $Na_{0.68}WO_3$ for $x=0.25$ and 0.68 after background subtraction.

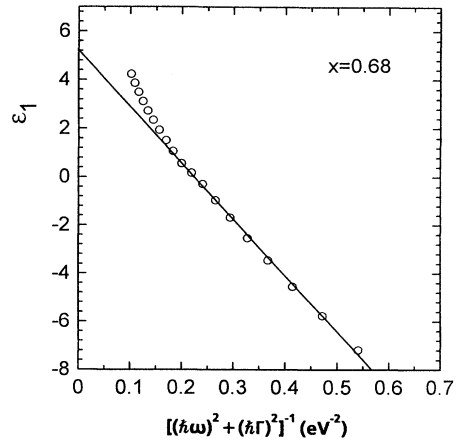

FIG. 3. A plot of ϵ_1 of $Na_{0.68}WO_3$ vs $[(\hbar\omega)^2+(\hbar\Gamma)^2]^{-1}$ for small $\hbar\omega$ to determine the background dielectric constant ϵ_∞.

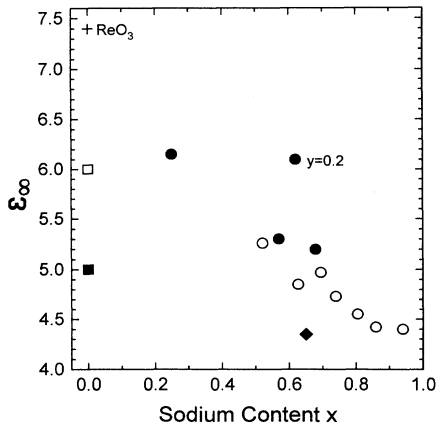

FIG. 4. The background dielectric constant ϵ_∞ of cubic Na_xWO_3 and compensated $Na_xTa_yW_{1-y}O_3$. Solid circles: values derived from EELS data (present work); open circles: from optical ellipsometry in the energy region of the volume plasmon (Ref. 25); solid diamond: from optical reflectivity (Refs. 18 and 23). For comparison we present optical data for the related cubic compound ReO_3 (crosses) (Ref. 60); for monoclinic WO_3 values from ellipsometry data (Ref. 25) (solid squares) and from the refraction index (Ref. 59) (open squares), where ϵ_∞ is calculated from the mean value over the three crystal axes.

well with those from HREELS (Ref. 14) and optical measurements[25] but they are by a factor of approximately 0.45 lower than effective masses deduced from the conduction-band shape in PES (Ref. 14) and from magnetic susceptibility data.[28]

Figure 6 shows the O 1s absorption edges for monoclinic reduced $WO_{3-\delta}$ and Na_xWO_3 after background subtraction which reflect the density of unoccupied O 2p states. For all concentrations the onset appears at 529.2 eV, followed by a first peak with a maximum at 531.0 eV and a subsequent intensity minimum at 533.8 eV. Further maxima are observed for $WO_{3-\delta}$ at 538.0, 541.5, and 544.8 eV. With increasing Na content these structures narrow and are shifted to lower energies. For $x=0.25$ they lie at 537.5, 540.2, and 544.4 eV; for $x=0.68$ they occur at 537.0, 539.5, and 543.8 eV. The intensity of the feature at about 540 eV clearly increases with increasing Na content. In Fig. 7(a) we present the width (FWHM) of the first peak in the O 1s spectra as a function of x. With increasing x the width decreases from 2.32 eV for $x=0.25$ to 1.94 eV for $x=0.68$. For comparison we also include the corresponding value for $WO_{3-\delta}$ having a higher width of 2.61 eV. Figure 7(b) shows the splitting

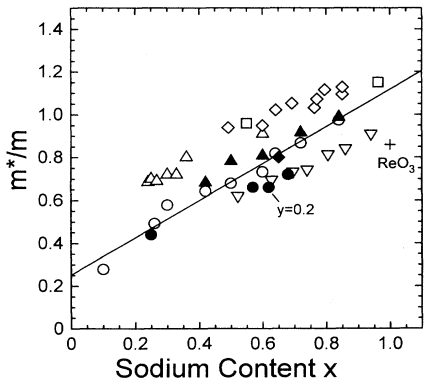

FIG. 5. Effective masses of the conduction-band electrons of cubic ($x>0.2$) Na_xWO_3 and $Na_xTa_yW_{1-y}O_3$, and tetragonal ($x=0.1$) Na_xWO_3. Solid circles: values derived from EELS data (present work); open down triangles: from optical ellipsometry (Ref. 25); filled diamond: from optical reflectivity (Refs. 18 and 23); open circles: from HREELS measurements (Refs. 14 and 20); filled up triangles: from high-resolution PES (Refs. 13 and 14); open up triangles (Ref. 27), open squares (Ref. 28), and open diamonds (Ref. 28): from magnetic susceptibility measurements; cross: from the optical reflectivity of ReO_3 (Ref. 60). Note that the values of the PES and magnetic susceptibility effective masses are much lower than those of Refs. 14 and 28, respectively (see Sec. V B). The solid line is a linear fit to the HREELS data.

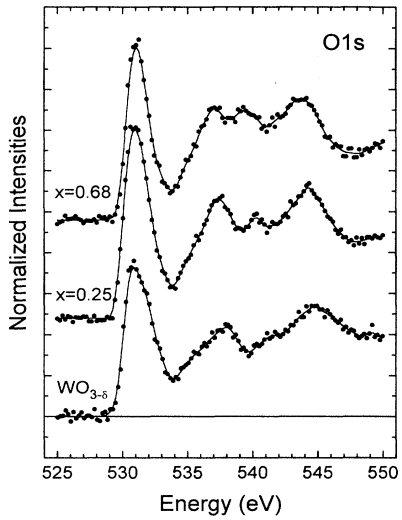

FIG. 6. The O 1s absorption edges of $WO_{3-\delta}$, $Na_{0.25}WO_3$, and $Na_{0.68}WO_3$ after background subtraction.

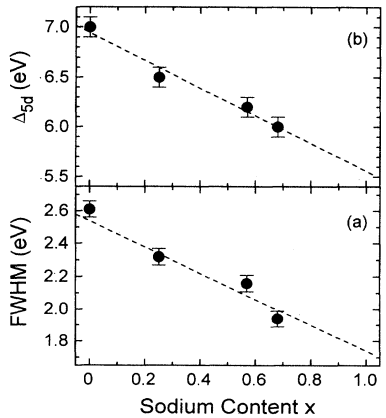

FIG. 7. (a) The width (FWHM) of the first peak in the O 1s absorption edge and (b) the crystal field splitting Δ_{5d} between the t_{2g} and e_g bands of cubic Na_xWO_3 as a function of sodium content x. The values for $x=0$ correspond to monoclinic $WO_{3-\delta}$. The dashed lines are guides to the eye.

Δ_{5d} between the maximum of the first peak in the O 1*s* spectra and the maximum of the following structure at about 537 eV. This band splitting decreases simultaneously with the width of the first peak.

B. Dispersion of the charge carrier plasmon

In Fig. 8(a) we show the loss function in the region of the charge carrier plasmon of $Na_{0.68}WO_3$ for momentum transfer q up to 0.6 Å^{-1} parallel to the (100) direction. The dispersion of the volume plasmon, indicated by the dashed-dotted line, is clearly positive. Maxima occur between 2.1 eV ($q=0.1$ Å^{-1}) and 2.7 eV ($q=0.6$ Å^{-1}). For $q \leq 0.15$ Å^{-1} an additional structure appears on the low-energy side of the volume plasmon due to surface plasmon excitations. The reason for the surface plasmon $\hbar\omega_S$ to occur at nearly the same energy as the bulk excitation $\hbar\omega_P$ is the relatively high background dielectric constant $\epsilon_\infty=5.2$. This leads to a ratio of the surface plasmon to the volume plasmon energy of $[\epsilon_\infty/(\epsilon_\infty+1)]^{1/2}=0.92$. Therefore, surface and bulk plasmons overlap. Surface plasmon excitations lying at energies comparable to the screened volume plasmon energy have already been detected with EELS in reflection.[14,18,19] At $q \geq 0.4$ Å^{-1} an additional peak at 2.1 eV is observed which is due to double scattering by an excitation of a plasmon with $q=0$ and a phonon with q equal to that set by the spectrometer.[55]

In Fig. 9(a) the energies $\hbar\omega(q)$ of the maxima of the volume plasmon peaks are plotted versus the squared momentum transfer q^2. As expected the dispersion is quadratic in q for low momentum transfer. In order to fit a function of the form $\omega(q)=\omega_P+Aq^2$ to the plasmon maxima only data from 0.14 Å^{-1} up to $q_c=0.28$ Å^{-1} were used. This avoids inaccuracies in the determination of the dispersion coefficient α due to the surface plasmon appearing at low q and due to q^4 contributions at high q. The fit parameters are then $\hbar\omega_P=(2.11\pm0.01$ eV and $\hbar A=(2.07\pm0.17)$ eV Å^2, leading to $\alpha=0.20\pm0.02$ via Eq. (2a). Above q_c the dispersion of the maximum becomes weaker. Contributions from possible q^4 terms in the series expansion of $\hbar\omega(q)$ could not be detected below q_c. When regarding three NFE bands it is also reasonable to apply the same fitting region, e.g., $q \leq q_c$, because

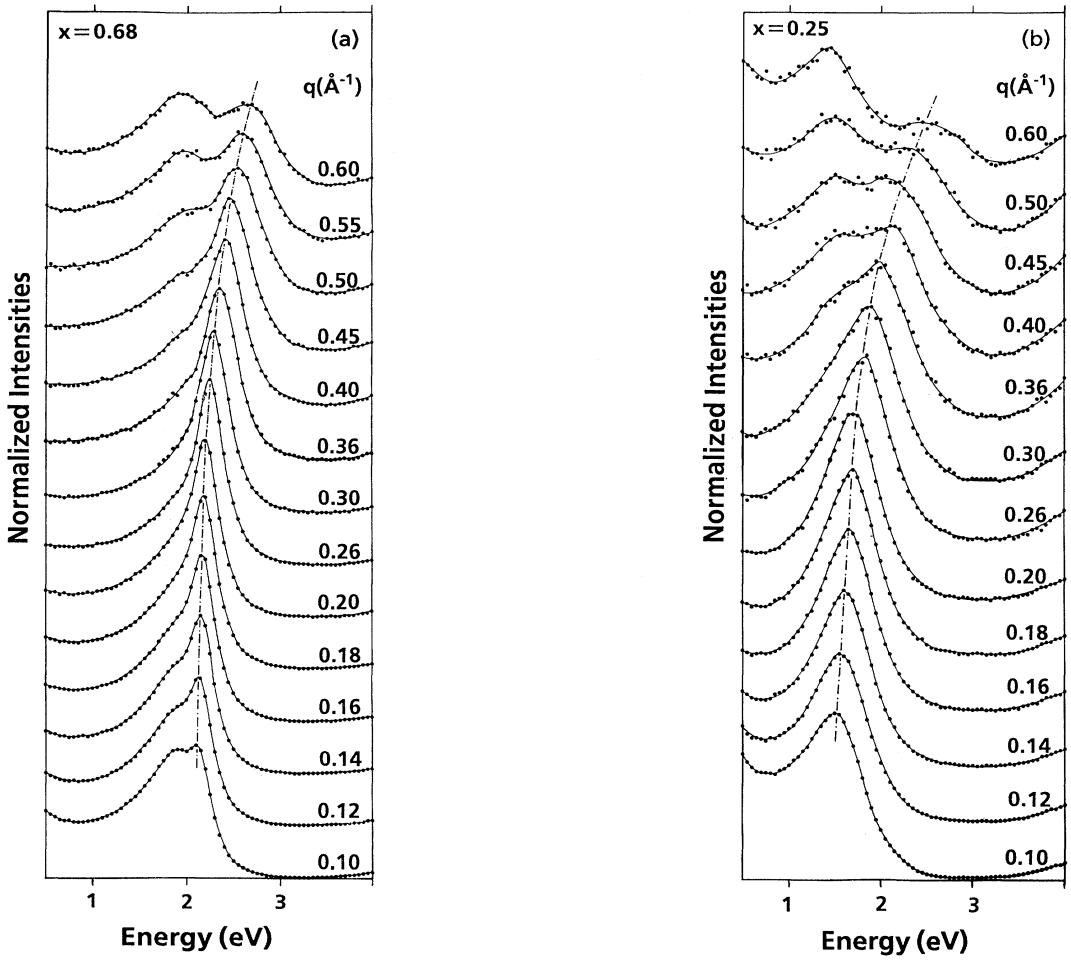

FIG. 8. The measured low-energy loss spectrum of Na_xWO_3 as a function of momentum transfer q for different sodium content: (a) $x=0.68$ and (b) $x=0.25$. The dispersion of the volume plasmon is indicated by the dashed-dotted line. A surface plasmon excitation is visible at low q on the low-energy side of the volume plasmon. At high q double scattering creates a peak occurring at the plasmon energy for $q=0$.

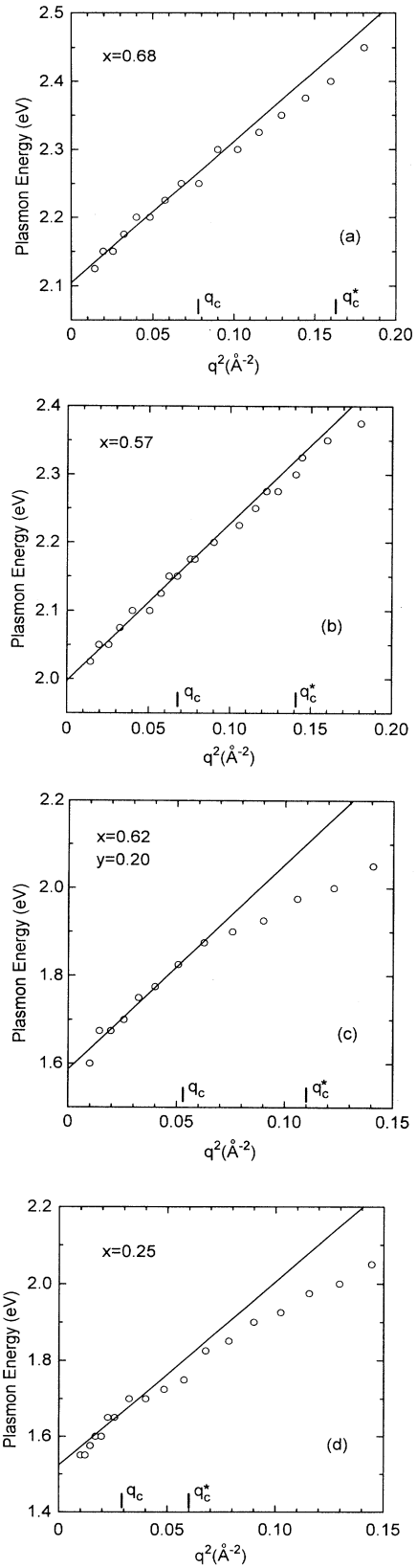

FIG. 9. The dispersion of the maximum of the volume plasmon excitation of Na_xWO_3 vs q^2: (a) $x=0.68$; (b) $x=0.57$; (c) $x=0.62$, $y=0.20$; (d) $x=0.25$.

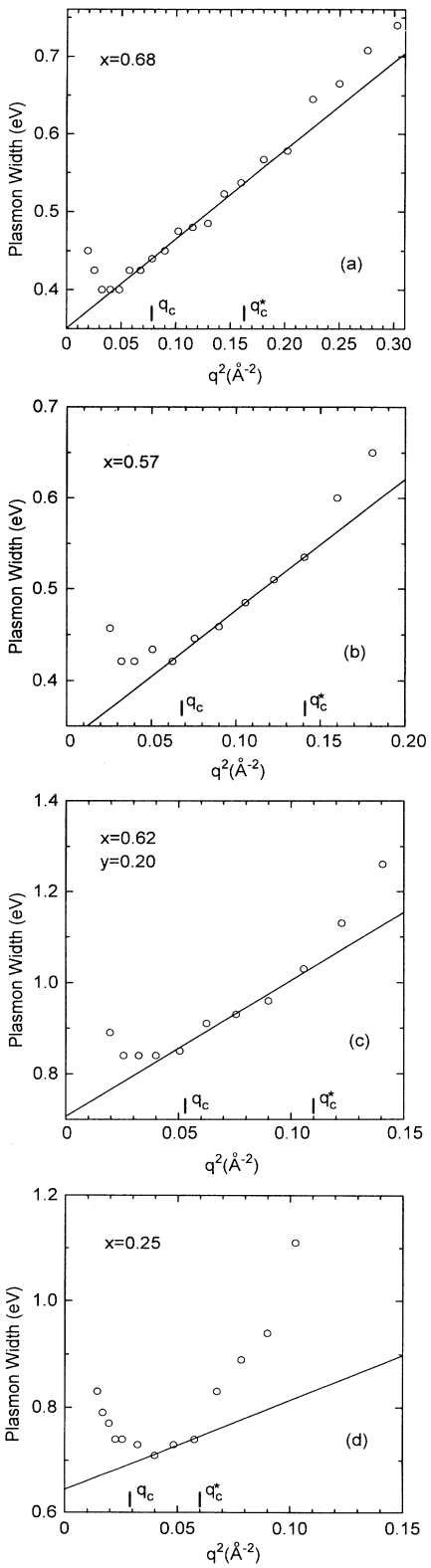

FIG. 10. The width (FWHM) of the volume plasmon peak of Na_xWO_3 vs q^2: (a) $x=0.68$; (b) $x=0.57$; (c) $x=0.62$, $y=0.20$; (d) $x=0.25$. The apparent increase below $q \leq 0.17$ Å^{-1} is due to the rather large intensity of the surface plasmon lying at nearly the same energy as the volume plasmon. Above q_c^* the width increases due to the onset of Landau damping.

q_c is lower than q_c^*.

Looking at the dispersion of the volume plasmon width versus q^2 in $Na_{0.68}WO_3$ [see Fig. 10(a)] an increase below approximately $q \sim 0.17$ Å^{-1} apparently seems to occur. This is probably an effect of the difficulty in estimating the exact contribution of the surface plasmon in this low q region. Near $q \sim 0.2$ Å^{-1} the width reaches a minimum value of $\Delta E_{1/2}(0.2\ \text{Å}^{-1}) = 0.40$ eV, increasing then linearly with q^2 up to $q \sim 0.45$ Å^{-1}. A fit with the function $\Delta E_{1/2}(q) = \Delta E_{1/2}(0) + Bq^2$ in this q region yields $\Delta E_{1/2}(0) = 0.35$ eV and $B = (1.14 \pm 0.06)$ eV Å^2. In order to determine the width at higher q values the contribution of the 2.1-eV peak due to the double scattering process mentioned above has been subtracted. Above $q \sim 0.45$ Å^{-1}, which is of the order of the critical wave vector $q_c^* = 0.40$ Å^{-1} in the case of three NFE bands, the width increases more rapidly due to the onset of Landau damping.

Qualitatively, the preceding description of the plasmon dispersion in $Na_{0.68}WO_3$ is also valid for the lower dopant concentrations. We therefore present these results more briefly. As an example for loss data from samples with low dopant concentrations we show in Fig. 8(b) the momentum-dependent loss function in the energy region of the charge carrier plasmon for $x = 0.25$. For $x = 0.57$ and 0.25 and the Ta-compensated sample, the plasmon dispersion and the dispersion of the plasmon width are again shown in Figs. 9(b)–9(d) and 10(b)–10(d), respectively. A summary of the evaluated data is given in Table I. With decreasing x the plasmon energy $\hbar\omega(q=0)$ is reduced, the dispersion coefficient α is slightly increased, and there is an increasing plasmon width $\Delta E_{1/2}$. Because of the larger width at lower x-y, it is difficult to separate surface plasmons and volume plasmons at low momentum transfer.

For one dopant concentration ($x = 0.57$) we have tried to measure the anisotropy of the plasmon dispersion. Along two different directions of the momentum transfer q parallel to (100) and (110) no statistically significant difference could be found.

V. DISCUSSION

A. Excitations at small momentum transfer

The observed energies of the VP excitation between $\hbar\omega_P = 1.52$ eV ($x = 0.25$) and $\hbar\omega_P = 2.11$ eV ($x = 0.68$) correspond to plasma edges observed in reflectivity measurements.[23] The energies are considerably lower than their free-electron values, e.g., $\hbar\Omega_P = 2.50$ eV for $x = 0.25$ and $\hbar\Omega_P = 4.07$ eV for $x = 0.68$, respectively, due to a rather high background polarizability leading to a background dielectric constant ϵ_∞ of the order of 5–6. These x-dependent ϵ_∞ values are consistent with those determined from optical ellipsometry data[25] (see Fig. 4), thus confirming that our surface plasmon subtraction procedure was reasonable. However, slight differences that appear for ϵ_∞ are probably due to remaining uncertainties in this surface plasmon correction especially at low x-y where surface and bulk plasmons are more difficult to separate.

Above $\hbar\omega \sim 2.3$ eV the dielectric function cannot be described anymore by a simple Drude model with a frequency-independent background dielectric constant ϵ_∞ due to contributions of the IB peak.[25] The maximum of this peak appears at $\hbar\omega = 4.1$ eV ($x = 0.68$) in ϵ_2, which is lower than values observed in optical ellipsometry, $\hbar\omega \sim 4.9$ eV ($x = 0.695$) (Ref. 25) and $\hbar\omega \sim 4.55$ eV ($x = 0.72$) (Ref. 24), and the value derived from optical reflectivity, $\hbar\omega \sim 4.6$ eV ($x = 0.65$) (Ref. 23), for comparable sodium content. In the isoelectronic compound ReO_3 this IB peak appears in ϵ_2 derived from reflectivity data at 4.2 eV.[60] A shift of this IB peak in ϵ_2 to lower energies with decreasing sodium content of the order of about 0.2 eV on going from $x \sim 0.7$ to $x \sim 0.5$ is observed in optical ellipsometry measurements[24,25] which is comparable with the 0.3-eV shift in ϵ_2 between the EELS results for $x = 0.68$ and 0.25, although for $x = 0.68$ and 0.57 and the Ta-compensated sample no difference is observed. This might be an artifact resulting from inaccuracies in the fitting and correction procedure. The zero crossing of ϵ_1 at $\hbar\omega = 2.05$ eV for $x = 0.68$ does not differ much from the optical data, yielding 2.3 eV for $x = 0.695$,[25] 2.1 eV for $x = 0.72$,[24] and 2.0 eV for $x = 0.65$.[18,23]

Another quantity that can be compared with optical data is the width $\Delta E_{1/2}(0)$ of the plasmon line at $q = 0$, extrapolated from the region where $\Delta E_{1/2}(q)$ varies linearly with q^2. Correcting $\Delta E_{1/2}(0)$ values (see Table I) for experimental resolution (160 meV) and assuming for simplicity Gaussian shapes we obtain the corrected values 0.31 eV for $x = 0.68$, 0.29 eV for $x = 0.57$, 0.69 eV for the Ta-compensated sample, and 0.62 eV for $x = 0.25$. The value of $\Delta E_{1/2}(0) \sim 0.3$ eV for the two higher doped tungsten bronzes is again in good agreement with damping parameters $\hbar\Gamma = 0.315$ eV derived from optical reflectivity[23] via a Drude model for an $x = 0.65$ crystal.[18] Observed widths of a surface plasmon excited with EELS in reflection are of the same order, 0.35 eV (corrected for experimental resolution) for $x = 0.61$ and 500 eV incident beam energy,[18] and 0.29 eV for $x = 0.7$ and 100 eV incident beam energy.[61] Optical damping parameters $\hbar\Gamma$ from a Drude fit on ellipsometry data are $\hbar\Gamma \sim 0.20$–0.24 eV (Ref. 25), and $\hbar\Gamma \sim 0.32$–0.64 eV (Refs. 24 and 62) for $0.7 > x > 0.5$. For ReO_3 a Drude fit to optical reflectivity data yields $\hbar\Gamma = 0.225$ eV (Ref. 60), but for a surface plasmon a rather high width of $\hbar\Gamma = 0.60$ eV (measured at 500 eV incident beam energy and corrected for experimental resolution) was observed.[18]

The broad feature in the loss function (see Fig. 1) between about 15 and 30 eV can be attributed to a plasmon of all 18 σ and π valence electrons. The corresponding plasmon frequency would be 21 eV for $x = 0.68$. The increase of the loss function at about 11 eV is due to an interband transition showing a maximum in ϵ_2 at 10 eV. An assignment of the several structures appearing in the loss function at 9, 12,2, 13.7, 15.6, 20, 22.5, 25.6, and ~32 eV (see Fig. 1) is rather difficult because they lie close together. Langell and Bernasek[19] found in their EELS in reflection spectrum for an $x = 0.91$ sample only four of these excitations in that region, at 12.9, 15.6, 20, and 22 eV, and an additional structure at 29 eV. The

latter might correspond to the weak shoulder at ~32 eV in the present loss function shown in Fig. 1.

Starting from the valence-band maximum at 4.4 eV below E_F three maxima lying at about 10.5 eV, 21–22 eV, and 27–28 eV, and a weak hump at 16 eV final-state energy above E_F have been observed in constant initial state (CIS) spectroscopy[10] for $x=0.5$. The corresponding transition energies are then 14.9, 25.4–26.4, 31.4–32.4, and 20.4 eV for the weak hump which were assigned to transitions from O $2p$ states to empty d states.[10] These energies are similar to the present structures at 13.7, 25.6, ~32, and 20 eV. Comparing their results with x-ray induced PES on O_2 in the gas phase, Langell and Bernasek[19] attribute their 22-eV peak to an O $2s$ core-level excitation.

The 0.24-eV shift of the Na $2p$ core-level excitation to higher energy in the $x=0.25$ sample also appears for all other high-energy excitations ($\hbar\omega \geq 5$ eV) in the loss spectrum. This simultaneous shift is an argument against a change of the oxidation number of sodium near the metal-nonmetal transition at $x \sim 0.2$. An admixture of sodium orbitals to the conduction band near $x \sim 0.2$ was derived from NMR Knight shifts and enhanced spin-lattice relaxation times.[6,7,9] However, this should result in a shift of the Na $2p$ excitation to lower energy. The constant shift of all levels in the $x=0.25$ crystal might indicate a higher band gap due to the beginning of a structural phase transition being connected with the metal-nonmetal transition in the cubic Na_xWO_3 crystals at $x \sim 0.2$. This may indicate some tetragonal distortion for this concentration. The x-ray powder pattern for the $x=0.25$ sample shows very weak additional structures near the (100) peak.

The onset at 529.2 eV in the O $1s$ absorption edge spectra (Fig. 6) of Na_xWO_3 corresponds to the Fermi level for the unoccupied states of the conduction band broadened by the energy resolution of 0.4 eV. An interpretation of the several structures appearing in the O $1s$ absorption edge spectra can be obtained by comparing the present data with the band-structure calculations[35] for monoclinic WO_3 and Na_1WO_3 and also with the O $1s$ absorption edges of TiO_2 (an oxide with completely unoccupied $3d$ states) and $BaTiO_3$ (a perovskite) measured with x-ray absorption spectroscopy.[63] In the Ti compounds the Ti $3d$ states are split into t_{2g} and e_g bands by the octahedral crystal field. Further structures above 536 eV extending up to about 18 eV above the onset of the O $1s$ edges were attributed to Ti $4s$ and $4p$ states hybridized with O $2p$ states. For $BaTiO_3$ the spectrum is more complex with additional intensity at $\hbar\omega \sim 537$ eV, presumably due to Ba $6s$ states. The crystal field splitting is also present in Na_xWO_3 and we therefore assign the first two O $1s$ peaks lying at 531 and ~538 eV to t_{2g} and e_g states, respectively, which are hybridized with O $2p$ states. For the undoped WO_3 the region above 540 eV, also extending up to about 18 eV above the onset of the O $1s$ edge, then maps the density of W $6s$ and $6p$ states admixed to O $2p$ states. For the doped Na_xWO_3 additional intensity appears with increasing x at about 540 eV which can be attributed to Na $3s$ states which are expected to be somewhat higher in energy relative to E_F than Ba $6s$ states in $BaTiO_3$. The energy of these Na $3s$ states relative to the Fermi level is then ~11 eV for $x=0.25$ and ~10 eV for $x=0.68$. This is in very good agreement with Bullet's LCAO band-structure calculation[35] for Na_1WO_3 where sodium orbitals contribute to the unoccupied density of states mainly at ~12 eV above the Fermi level.

The width of the t_{2g} peak, e.g., the unoccupied part of the conduction band, decreases with increasing x [see Fig. 7(a)]. Together with the nearly constant width of the occupied part this supports a model of conduction-band narrowing with increasing x in Na_xWO_3 as proposed by Egdell and Hill.[13,14] This is also consistent with the fact that the effective mass increases with increasing x. The explanation given by Goodenough is that Na competes for bonding to the O $2p$ states and thus the O $2p$–W $5d$ interaction decreases with increasing Na content.[33] The O $2p$–W $5d$ interaction produces the t_{2g} bandwidth and gives the crystal field splitting Δ_{5d} of the t_{2g} and e_g bands which also decreases with increasing sodium content x [see Fig. 7(b)]. This crystal field splittings $\Delta_{5d}=7$ eV (WO_3) and $\Delta_{5d}=6$ eV ($x=0.68$) are higher than in TiO_2 ($\Delta_{5d}=2.6$ eV) and in $BaTiO_3$ ($\Delta_{5d}=2.8$ eV).[63] Generally, an increase of crystal field splittings is expected as the oxidation state is increased [Ti(IV)→W(VI)] and as going from the first transition series to the third.

In Bullet's LCAO band-structure calculations[35] for Na_1WO_3 the overall width of the conduction band is 2.6 eV, having a sharp peak in the density of states at about 1.65 eV above the bottom of the band. The Fermi energy ($E_F \sim 1.1$ eV) derived from this calculation is comparable with the x-independent width (1 eV) of the occupied part of the t_{2g} bands measured with high-resolution PES.[14] Subtracting $E_F=1.1$ eV from the theoretical 2.6-eV conduction-band width we obtain 1.5 eV ($x=1$) for the unoccupied part. The width (FWHM) [Fig. 7(a)] of 1.94 eV for $x=0.68$ of the first peak in the O $1s$ absorption edge is comparable with this value. However, the full width at the bottom of the peak which should be compared with the calculated density of states has a value of approximately 3.5 eV for $x=0.68$, much higher than the calculated value even if the experimental resolution of 0.4 eV is taken into account. According to the LCAO band-structure calculation of Bullet[35] for $x=1$ the e_g bands lie 2.5 eV (onset) above the bottom of the Fermi level and have a width of about 4.25 eV. In the experiment the onset of the feature corresponding to the e_g bands is shifted to approximately 5 eV above E_F and has a width of about 5 eV. These differences between the band-structure calculations[34,35] and experimental results have already been observed in PES (Refs. 10, 11, and 14) for the width of the occupied valence band and in inverse PES (Ref. 17) for the width of the unoccupied part of the conduction band.

A quantitative comparison of the EELS O $1s$ absorption edges with inverse PES measurements[17] is rather difficult. In the inverse PES experiment for $x=0.64$ (Ref. 17) a peak at about 2.8 eV and a very broad feature at ~5.5 eV above the Fermi level are observed, but they

lie on a strongly rising background. The position of the first structure is consistent with the maximum of the first peak in the O 1*s* absorption edge, 1.8 eV above E_F, when a shift due to the strong background is taken into account. The second one probably corresponds to the second peak in the O 1*s* absorption edge, the maximum of which lies 7.8 eV ($x=0.68$) above E_F (see Fig. 6).

B. The dispersion of the charge carrier plasmon

For all Na concentrations, a dispersion of the charge carrier plasmon has been observed which is quadratic in momentum transfer q. In general not only terms proportional to q^2 but also higher-order terms, e.g., proportional to q^4, are expected in the series expansion of $\hbar\omega(q)$.[45] However, within error bars, no term proportional to q^4 could be detected for the sodium-tungsten bronzes, contrary to previous investigations on simple metals.[64–66] This can be explained by a rule given by Sturm[67] which states that the quadratic dispersion is a good approximation for $(q/k_F)^2<0.1$. For the bronzes investigated here this region corresponds to $q\leq 0.16$ Å^{-1} and $q\leq 0.22$ Å^{-1} for $x=0.25$ and $x=0.68$, respectively. These values are close to the critical momentum transfers q_c in these systems up to which data were used to fit a quadratic dispersion. Therefore, a negligible q^4 term should be expected below q_c. Furthermore, estimating the ratio R of the q^4 term to the q^2 term from the series expansion for $\hbar\omega(q)$ given by Sturm[45] and taking into account the reduction of E_F and k_F when considering three identical parabolic bands (see Sec. II), we obtain $R<7.5\%$ for the q ranges given above. Thus, q^4 contributions are lower than ~ 15 meV within the fitting region and therefore negligible.

The measured dispersion coefficient α for the sodium-tungsten bronzes are about $\frac{1}{4}$ of the dispersion coefficients α_{RPA} derived in the framework of RPA for a system with one parabolic conduction band (see Fig. 11). For the Ta-compensated bronze the measured α is about $\frac{1}{2}$ of α_{RPA}. There is an extensive debate in the literature on models which can explain in a reduction of the plasmon dispersion compared to that calculated in the mean-field RPA theory.[45,48,53,68–75]

Firstly, the small dispersion coefficients could be explained in the framework of a free-electron model by exchange and correlation effects which for higher r_s values, i.e., lower electron densities, should lower α [see Eq. (3)]. In Al (Ref. 66), Na (Ref. 65), and K (Refs. 64 and 65) a reduction of the dispersion coefficient has been observed (see Fig. 11) which could be explained by a reasonable static local field correction function $G(q,0)$.[65] For the heavier alkali metals Rb and Cs, having higher r_s values, nearly no dispersion and a negative dispersion had been detected, respectively, which could not be explained by present many-body theories on exchange and correlation effects.[64,65] Lipparini *et al.*[74] have calculated the influence of multipair excitations to sum rules yielding a dispersion coefficient close to zero for r_s values close to that of Cs (see Fig. 11).

On the other hand, Aryasetiawan and Karlsson[75] have recently shown that band-structure effects, which become more and more important when going from Na to Cs, cause the negative plasmon dispersion in Cs.

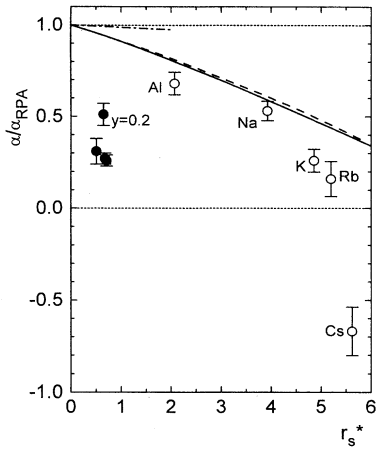

FIG. 11. The volume plasmon dispersion coefficient α of the sodium-tungsten bronzes Na_xWO_3 ($x=0.68$, 0.57, and 0.25) (solid circles) and $Na_{0.62}Ta_{0.2}W_{0.8}O_3$ normalized to the RPA value vs the effective density parameter $r_s^*=(m^*/\epsilon_\infty)r_s$. Note that the value for the bronze with the highest doping is placed on the *right*-hand side. Included for comparison are results for Al (Ref. 66) and the alkali metals (Ref. 64 and from Table I of Ref. 65) for which $r_s^*\sim r_s$. The solid line is the Vashishta-Singwi (VS) (Ref. 76) static local field correction ($r_s^*=r_s$), the dashed line a dynamical extension (Refs. 64, 65, and 77). An estimation of local field corrections for the tungsten bronzes ($m^*/\epsilon_\infty\approx 0.1$) within the theory of VS is indicated by the dashed-dotted line near $\alpha/\alpha_{\mathrm{RPA}}=1$.

Since in the sodium-tungsten bronzes the conduction-band electron densities are rather small ($r_s\sim 5$–7), corresponding to r_s values which are even higher than those of Cs ($r_s=5.8$), it is tempting to explain the small dispersion coefficients in Na_xWO_3 by exchange and correlation effects. However, on looking more carefully, the r_s values should be strongly renormalized due to the low effective masses of the order of $m^*\sim 0.6$ m and the high background dielectric constants $\epsilon_\infty\sim 5.5$. Both lead to a reduction of the r_s values to give effective density parameters $r_s^*\sim 0.7$–0.5. This reduction occurs by replacing e^2 by e^2/ϵ_∞ and m by m^* in all formulas. The strong shielding of the Coulomb repulsion by the background dielectric constant leads to a reduction of the ratio between mean potential energy per electron to its mean kinetic energy and, therefore, we are again in the weak coupling regime where the RPA should work. Therefore, in this approximation for a free-electron system, for Na_xWO_3 we should expect dispersion coefficients which are close to the RPA values and not strongly reduced by exchange and correlation effects.

However, the above discussion holds only for a free-electron system with an effective mass m^*. When regarding the band-structure calculations,[34,35] the conduction band is not a simple parabolic band with an effective mass but it is composed out of three t_{2g} bands. In Sec. II,

we have already considered the effect of replacing one parabolic conduction band by three identical parabolic bands which is of course an oversimplified picture. According to Eq. (4) the theoretical dispersion coefficient is reduced by a factor of $(1/3)^{2/3}=0.48$. In this way the discrepancy between experiment and theory is significantly reduced (see Table III). But apart from the Ta-compensated sample for which $\alpha_{exp}=1.08\alpha_{th}$, the experimental α_{exp} values are still smaller than the theoretical α_{th} values for this simple three-NFE-band model, $\alpha_{exp}/\alpha_{th}=0.65$ for $x=0.25$, 0.57 for $x=0.57$, and 0.56 for $x=0.68$.

Another apparent contradiction can be resolved using the three-NFE-band model. High-resolution PES data[14] provide directly the width of the occupied part of the conduction band as roughly 1 eV independent of sodium content x and in agreement with the concentration-dependent semiempirical LCAO model of Wolfram and Sutcu.[41] From m^*, derived from the present EELS data on ω_P and ϵ_∞ and from the electron density n, one obtains $E_F=\hbar^2k_F^2/(2m^*)\sim 2.3$–$2.7$ eV by assuming one band only. But for the three-NFE-band model this value is reduced again by the same factor 0.48 resulting in a width of the occupied part of the conduction band of 1.1–1.3 eV close to the PES and LCAO model results. Vice versa, the effective masses determined here ($m^*/m=0.44$–0.78) are in agreement with the results from optical investigations[18,23,25] but are smaller by a factor of 0.45 than those determined from PES data.[13,14] In that case, effective masses were deduced from the PES conduction-band shape by assuming one band only via $E_F=\hbar^2k_F^2/(2m^*)\sim 1$ eV.[13,14] E_F being fixed one obtains $k_F^2\propto m^*$ which in the three-band case reduces the effective masses again by the same factor 0.48, which is nearly the same factor as the apparent deviation of 0.45 between EELS and PES effective masses when evaluating the PES data incorrectly within the one-band model.

Measurements of the electronic specific heat[26,27] of cubic Na_xWO_3 ($x>0.2$) show a nearly linear dependence of the low temperature specific heat coefficient $\gamma_e\propto D(E_F)$ on x. This could not be explained by a NFE model with an x-independent effective mass ($m^*/m=1.6$) (Ref. 27). Within our three-NFE-band model, neglecting electron-phonon interaction, we get $D(E_F)=3D_i(E_{Fi})$, with $D_i(E_{Fi})\propto m^*q_{Fi}$ being the density of states at the Fermi level in the ith band. Calculating γ_e in this way using x-dependent effective mass values as deduced from HREELS data[14] for which the widest range of x has been investigated we achieve an excellent agreement with the experimental values (see Fig. 12) and also with the LCAO results of Wolfram and Sutcu.[41] γ_e then is proportional to $m^*(x)x^{1/3}$ which behaves nearly linear for $0.1<x<1$. A linear dependence of $D(E_F)$ on x was also found in PES.[13,14]

Furthermore, estimating x-dependent effective masses within the three-NFE-band model from measurements of the magnetic susceptibility χ_e (Refs. 27 and 28) with the NFE relation $\chi_e=\mu_B^2D(E_F)[1-\frac{1}{3}(m/m^*)^2]$, which probably oversimplifies the diamagnetic contribution, we obtain m^* values which are in reasonable agreement with corrected PES,[13,14] optical,[18,23,25] HREELS,[14,20] and EELS results (see Fig. 5). The three-cylinder LCAO model of Wolfram and Sutcu also is consistent with experimental χ_e values.[41]

A quadratic dependence of the plasmon linewidth $\Delta E_{1/2}=\Delta E_{1/2}(0)+Bq^2$ for low momentum transfer q is generally expected for simple metals[47] and mainly results from the decay of plasmons via interband transitions.[46] However, the heavy alkali metals Rb and Cs show a weaker dispersion proportional to $q^{1.5}$ and q, respectively.[64,65] We observe a quadratic behavior in the case of the sodium-tungsten bronzes (Fig. 10) with $B=1.14$ eV Å^2 for $x=0.68$ up to $B=4.08$ eV Å^2 for $x=0.25$ (see Table I), values which are comparable with those reported for other simple metals like Al,[78] K,[64,65] and Na.[65] A strong increase of the plasmon linewidth due to the onset of Landau damping is consistent with critical wave vectors q_c^* determined within the three-NFE-band model while q_c values appear to be too low (see Fig. 10). On the other hand, q_c^* values instead of q_c are still consistent with deviations from the quadratic plasmon dispersion which are not so pronounced, as in the case of the plasmon linewidth (see Fig. 9).

Thus, apart from the remaining smaller deviation in the case of the plasmon dispersion coefficient, a rather consistent description of different data and quantities is achieved by considering the existence of three bands already in its most simple way, i.e., three identical free-electron bands with effective mass m^*.

Actually, the conduction band consists of three t_{2g} bands with the following three Fermi surfaces[36] (in the considered range of sodium content): one is roughly a sphere, the second is a warped sphere, and these two arise from the overlap of three orthogonal and interconnected

TABLE III. The experimental dispersion coefficient $\hbar A$ of the sodium-tungsten bronzes compared with theoretical values calculated with one parabolic band, three parabolic bands, and with three 2D bands for the (100) and the (110) direction, respectively.

x	$\hbar A$ (eV Å^2) experiment	$\hbar A$ (eV Å^2) one NFE band	$\hbar A$ (eV Å^2) three NFE bands	$\hbar A$ (eV Å^2) three cylinders (100)...(110)
0.25	4.8(10)	15.64	7.51	6.04...4.54
x-y=0.42	4.68(20)	9.18	4.41	4.24...3.18
0.57	2.39(4)	8.90	4.27	4.55...3.41
0.68	2.07(17)	8.05	3.86	4.32...3.24

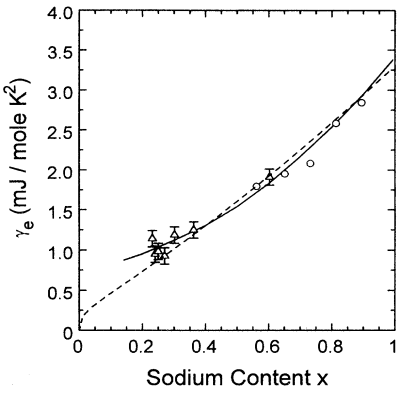

FIG. 12. The electronic contribution γ_e to the low-temperature specific heat (Refs. 26 and 27) of the conduction-band electrons of cubic Na_xWO_3. The solid line is a calculation based on our three-NFE-band model using effective masses from HREELS measurements (Ref. 14), the dashed line represents the results of the Wolfram and Sutcu LCAO model (Ref. 41).

cylinders which form the third Fermi surface. The model of three independent spheres can be regarded as one limiting case and the Wolfram-Sutcu model[41] with three independent cylinders as another one. We now apply the three-cylinder model, i.e., three independent two-dimensional (2D) bands, also to the plasmon dispersion evaluating the expressions given in the Appendix. We use a model which is simpler than the three-cylinder LCAO model considering that we only need the Fermi velocity in (A5) and (A6) and not the whole band structure. The three bands are roughly 2D sinusoidal bands with a filling (for the considered sodium concentrations) for which the 2D Fermi surface cross sections are nearly isotropic [the 2D $k_F=a^{-1}(2\pi x/3)^{1/2}$ is far from the Brillouin zone boundaries]. Then one can use for the Fermi velocity $v_F=(a/\hbar)W\sin k_F a$ where $2W$ is a measure of the bandwidth. To calculate the plasmon dispersion coefficient from (A5) and (A6), Eq. (A3) is required which in this model is given by

$$\langle v_q^2\rangle_{F,i}=\frac{1}{2}\frac{k_F v_F}{\pi\hbar a}\cos^2\Theta_i \ , \tag{9a}$$

$$\langle v_q^4\rangle_{F,i}=\frac{3}{8}\frac{k_F v_F^3}{\pi\hbar a}\cos^4\Theta_i \ , \tag{9b}$$

where i numerates the three cylinders and Θ_i is the angle between $\mathbf{q}$ and the cylinder normal in the plane fixed by $\mathbf{q}$ and the axis of the ith cylinder. With $\sum_i\cos^2\Theta_i=2$ we obtain then from (A5) and (A6)

$$\frac{\omega_P^2\epsilon_\infty}{4\pi e^2}=\frac{k_F v_F}{\pi\hbar a} \ , \tag{10}$$

$$2\omega_P A=\tfrac{3}{8}V_F^2 G(\mathbf{e}) \quad \text{with } G(\mathbf{e})=\sum_{i=1}^{3}\cos^4\Theta_i \ . \tag{11}$$

The bandwidth $2W$ is the only parameter of this model and is determined by means of Eq. (10) from the plasmon energy $\hbar\omega_P$ and the background dielectric constant ϵ_∞. Interpolation then gives the bandwidth $2W=2(2.75-3.76x+2.58x^2)$ eV. We thus find a narrowing of the bandwidth from 3.9 eV for $x=0.25$ up to 2.8 eV for $x=0.68$ in satisfactory agreement with experimental results, yielding 3.32 eV for $x=0.25$ and 2.94 eV for $x=0.68$, when taking the sum of the O 1s absorption edge width [see Fig. 7(a)] and the 1-eV PES conduction bandwidth.[14] However, the full width at the bottom of the O 1s peak which should be compared with the unoccupied part of the calculated density of states is of the order of 4 eV for $x=0.25$ and 3.5 eV for $x=0.68$. Adding the 1-eV PES conduction bandwidth this gives a width of 5 eV for $x=0.25$ and 4.5 eV for $x=0.68$ for the whole band which is much higher than the calculated values. Furthermore, Bullet's LCAO calculation[35] gives a conduction bandwidth of 2.6 eV for $x=1$. In the present three-cylinder model the Fermi energy varies between 0.5 and 0.8 eV which is less than the observed value of 1 eV.

The plasmon dispersion coefficient, Eq. (11), contains the anisotropy factor $G(\mathbf{e})$ with $G(100)=2$ and $G(110)=1.5$. This anisotropy would correspond to a plasmon energy difference at q_c of about 77 meV ($x=0.57$) which could not be detected experimentally. On the other hand, the anisotropy of the dispersion coefficient is too large to be negligible. In Table III the resulting dispersion coefficients A are given for both orientations and are to be compared with the experimental value showing no anisotropy. For $x=0.25$ the deviation of A from the experimental value is reduced further, but there is no significant difference to the three-NFE-band model for $x=0.57$ and 0.68. The strong anisotropy is probably overestimated within the three-cylinder model.

VI. CONCLUSION

We have determined the loss function, the dielectric function, x-dependent optical effective masses $m^*(x)$ and background dielectric constants $\epsilon_\infty(x)$, and Na 2p and O 1s absorption edges of cubic single crystalline Na_xWO_3 for $0.25\le x\le 0.68$ and the O 1s absorption edge of monoclinic $WO_{3-\delta}$. The dispersion of the charge carrier plasmon in the sodium-tungsten bronzes is positive quadratic for low momentum transfer q. We have demonstrated that the reduction of the plasmon dispersion coefficient compared to the free-electron RPA values is essentially determined by the threefold degeneracy of the conduction-band t_{2g} states in an octahedral field. On the other hand there remains a discrepancy between theory and experiment since the experimental values for $x=0.57$ and 0.68 are still roughly $\frac{2}{3}$ of the theoretically estimated ones. Such a deviation is not surprising since the plasmon dispersion, though an integral quantity, depends rather sensitively on details of the band structure due to the occurrence of the fourth power of the projection of the Fermi velocity on the plasmon propagation direction. Such details are lost within the simple three-NFE-band or three-cylinder model. There are further approximations which may lead to noncorrect plasmon dispersion

coefficients. We mention at first the neglect of local field effects in the crystal which are expected to play a role due to the localized character of the wave functions in question. Also not investigated is the role of the q dependence of the matrix element in the Ehrenreich-Cohen formula for the dielectric function. Furthermore, the second term in Eq. (A2) is neglected which can be more important for a complicated band structure. Also, both models used here are based on using $\omega_P^2\epsilon_\infty$ to fit band-structure data. So the dispersion coefficients depend rather sensitively on the determination of the background dielectric constant ϵ_∞. Moreover, low-lying interband transitions as observed in ReO_3 (Ref. 79) (which is isoelectronic to Na_1WO_3) have not been detected so far in the sodium-tungsten bronzes. If they are present they would also influence the plasmon dispersion. Finally, the influence of disorder of the Na atoms on the plasmon dispersion is unknown until now.

Within the three-NFE-band model x-dependent conduction-band effective masses $m^*(x)$ as determined from EELS, HREELS, optical ellipsometry, PES, specific heat, and magnetic susceptibility measurements are now consistent. m^* increases linearly with increasing sodium content. This conduction-band narrowing model is supported by the decreasing width of the unoccupied part of the conduction band while the width of the occupied part is nearly independent of x. Furthermore, with increasing x a reduction of the $t_{2g}-e_g$ ligand field splitting is observed. As the band narrowing, this can be explained by a decreasing O $2p$–W $5d$ interaction due to Na which competes for bonding to the O $2p$ states. Na $3s$ states lie 10–11 eV above the Fermi level.

From Na $2p$ core-level edges we conclude that there are no contributions from sodium orbitals to the conduction band close to the metal-nonmetal transition at $x\sim 0.2$ in Na_xWO_3. This result has also been derived from the PES measurements of Hill *et al.* However, below $x\sim 0.35$, an admixture of sodium orbitals to the conduction band was assumed to explain NMR Knight shifts and enhanced spin-lattice relaxation times.

ACKNOWLEDGMENTS

We thank R. v. Baltz and H. A. Romberg for their interest and helpful discussions. This work was performed within the research program of the Sonderforschungsbereich 195 supported by the Deutsche Forschungsgemeinschaft.

APPENDIX: PLASMON DISPERSION FOR A GENERAL BAND STRUCTURE

Nücker *et al.*[80] gave the systematic q expansion of the EC formula for the dielectric function for one band (neglecting the q dependence of the matrix element which will contribute also in the order q^2). Assuming a negligible imaginary part of the dielectric function, i.e., no essential interband transitions near the plasmon energy, their result for the plasmon dispersion (we use a slightly modified notation here and include ϵ_∞) is Eqs. (1a) and (1b) with

$$\frac{n}{m_{\rm opt}}=\langle v_q^2\rangle_F\ , \tag{A1}$$

$$A=\frac{2\pi e^2}{\epsilon_\infty\omega_P}\left\{\frac{\langle v_q^4\rangle_F}{\omega_P^2}+\frac{1}{12}\left\langle v_q\left[\frac{\mathbf{q}}{q}\cdot\frac{\partial}{\partial\mathbf{k}}\right]^2 v_q\right\rangle_F\right\}. \tag{A2}$$

$v_q=\mathbf{v}\cdot\mathbf{q}/q$ is the projection of the electron velocity $\mathbf{v}=\hbar^{-1}\partial\mathbf{E}/\partial\mathbf{k}$ on the plasmon propagation direction and in

$$\langle v_q^n\rangle_F=\frac{2}{(2\pi)^3}\int d^3k(-f')v_q^n=\frac{2}{(2\pi)^3}\int\frac{d^2k}{\hbar|\mathbf{v}|}v_q^n \tag{A3}$$

one has to integrate over the Fermi surface, f being the Fermi-Dirac distribution. The spin degeneration is included in (A3). Since $\langle v_q^0\rangle_F=D(E_F)$ is the density of states at the Fermi energy, Eq. (A3) can be rewritten as

$$\langle v_q^n\rangle_F=D(E_F)\overline{v_q^n}^F\ , \tag{A4}$$

where now the overbar with superscript F denotes the mean value at the Fermi energy. In general the second term in the dispersion coefficient (A2) will be much smaller than the first one due to the occurrence of higher derivatives and due to the prefactor and we therefore will neglect it. Then in the case of several conduction bands these expressions take the following form:

$$\frac{\omega_P^2\epsilon_\infty}{4\pi e^2}=\frac{n}{m_{\rm opt}}=\sum_i\langle v_q^2\rangle_{F,i}\ , \tag{A5}$$

$$2\omega_P A=\frac{\sum_i\langle v_q^4\rangle_{F,i}}{\sum_i\langle v_q^2\rangle_{F,i}}\ . \tag{A6}$$

Measurements of the loss function yield (in the present case x dependent) the plasmon frequency ω_P, the background dielectric constant ϵ_∞, and the dispersion coefficient A. These three quantities are connected with the band structure only in the rather complex integral form of the two Eqs. (A5) and (A6) and there is an additional connection between $m_{\rm opt}$ and ϵ_∞ due to the f-sum rule ($m_{\rm opt}$ is determined by the intraband transitions at the Fermi energy, ϵ_∞ by the interband transitions from all completely occupied bands to states above E_F, thus both depend on E_F). The form of the dispersion coefficient [see Eq. (4)] follows directly from (A6) since then for a parabolic band (A4) yields $\langle v_q^4\rangle_F\propto q_F^5\propto nE_F$. Equation (A6) also shows immediately that the same number of electrons distributed over several bands instead of one band gives a smaller A, since in the denominator one has the smaller power of the velocity. Finally we would like to mention that also in the case of a general band structure a dimensionless coefficient can be defined similarly to Eq. (2) by

$$A=\frac{\hbar}{m_{\text{opt}}}\alpha \quad \text{with } \alpha=\frac{n}{2\hbar\omega_P}\frac{\sum_i \langle v_q^4\rangle_{F,i}}{\left[\sum_i \langle v_q^2\rangle_{F,i}\right]^2} \tag{A7}$$

which in the case of only one conduction band takes on the form

$$\alpha_{1b}=\frac{n}{2\hbar\omega_P D(E_F)}\frac{\overline{v_q^4}^F}{(\overline{v_q^2}^F)^2}\ , \tag{A8}$$

where we made use of Eq. (A4).

---

*Present address: Institut für Festkörper- und Werkstoffforschung Dresden e.V., Institut für Festkörperforschung, Postfach 270016, D-01171 Dresden, Federal Republic of Germany.

†On leave from Department of Chemistry, University of Tokyo, Hongo, Bunkyo-Ku, Tokyo 113, Japan.

[1]For a review see J. P. Doumerc, M. Pouchard, and P. Hagenmuller, in *The Metallic and Nonmetallic States of Matter,* edited by P. P. Edwards and C. N. R. Rao (Taylor & Francis, London, 1985), p. 287.

[2]B. W. Brown and E. Banks, J. Am. Chem. Soc. **76**, 963 (1954).

[3]M. Atoji and R. E. Rundle, J. Chem. Phys. **32**, 627 (1960).

[4]P. J. Wiseman and P. G. Dickens, J. Solid State Chem. **17**, 91 (1976).

[5]W. A. Kamitakahara, B. N. Harmon, J. G. Taylor, L. Kopp, H. R. Shanks, and J. Rath, Phys. Rev. Lett. **36**, 1393 (1976).

[6]D. P. Tunstall, Phys. Rev. B **11**, 2821 (1975).

[7]B. R. Weinberger, Phys. Rev. B **17**, 566 (1978).

[8]W. Ramage and D. P. Tunstall, J. Phys. C **13**, 1623 (1980).

[9]D. P. Tunstall and W. Ramage, J. Phys. C **13**, 725 (1980).

[10]R. L. Benbow and Z. Hurych, Phys. Rev. B **17**, 4527 (1978).

[11]H. Höchst, R. D. Bringans, and H. R. Shanks, Phys. Rev. B **26**, 1702 (1982).

[12]G. Hollinger, F. J. Himpsel, B. Reihl, P. Pertosa, and J. P. Doumerc, Solid State Commun. **44**, 1221 (1982).

[13]R. G. Egdell and M. D. Hill, Chem. Phys. Lett. **85**, 140 (1982).

[14]M. D. Hill and R. G. Egdell, J. Phys. C **16**, 6205 (1983).

[15]G. Hollinger, P. Pertosa, J. P. Doumerc, F. J. Himpsel, and B. Reihl, Phys. Rev. B **32**, 1987 (1985).

[16]J. H. Davies and J. R. Franz, Phys. Rev. Lett. **57**, 475 (1986).

[17]P. M. G. Allen, P. J. Dobson, and R. G. Egdell, Solid State Commun. **55**, 701 (1985).

[18]R. E. Dietz, M. Campagna, J. N. Chazalviel, and H. R. Shanks, Phys. Rev. B **17**, 3790 (1978).

[19]M. A. Langell and S. L. Bernasek, Phys. Rev. B **23**, 1584 (1981).

[20]R. G. Egdell and M. D. Hill, Chem. Phys. Lett. **88**, 503 (1982).

[21]P. A. Cox and J. P. Kemp, Surf. Sci. **210**, 225 (1989).

[22]F. Consadori and A. Stella, Lett. Nuovo Cimento **3**, 600 (1970).

[23]D. W. Lynch, R. Rosei, J. H. Weaver, and C. G. Olson, J. Solid State Chem. **8**, 242 (1973).

[24]P. Camagni, A. Manara, G. Campagnoli, A. Gustinetti, and A. Stella, Phys. Rev. B **15**, 4623 (1977).

[25]J. F. Owen, K. J. Teegarden, and H. R. Shanks, Phys. Rev. B **18**, 3827 (1978).

[26]R. W. Vest, M. Griffel, and J. F. Smith, J. Chem. Phys. **28**, 293 (1958).

[27]F. C. Zumsteg, Phys. Rev. B **14**, 1406 (1976).

[28]J. D. Greiner, H. R. Shanks, and D. C. Wallace, J. Chem. Phys. **36**, 772 (1962); F. Kupka and M. J. Sienko, *ibid.* **18**, 1296 (1950).

[29]R. S. Crandall and B. F. Faughnan, Phys. Rev. B **16**, 1750 (1977).

[30]W. McNeill and L. E. Conroy, J. Chem. Phys. **36**, 87 (1962).

[31]P. A. Lightsey, D. A. Lilienfeld, and D. F. Holcomb, Phys. Rev. B **14**, 4730 (1976).

[32]M. A. Dubson and D. F. Holcomb, Phys. Rev. B **32**, 1955 (1985).

[33]J. B. Goodenough, Prog. Solid State Chem. **5**, 145 (1971).

[34]L. Kopp, B. N. Harmon, and S. H. Liu, Solid State Commun. **22**, 677 (1977).

[35]D. W. Bullett, J. Phys. C **16**, 2197 (1983); Solid State Commun. **46**, 575 (1983).

[36]L. F. Mattheiss, Phys. Rev. **181**, 987 (1969).

[37]H. R. Shanks, P. H. Sidles, and G. C. Danielson, Adv. Chem. Ser. **39**, 237 (1963).

[38]H. Höchst, R. D. Bringans, H. R. Shanks, and P. Steiner, Solid State Commun. **37**, 41 (1980).

[39]G. K. Wertheim and J. N. Chazalviel, Solid State Commun. **40**, 931 (1981).

[40]T. Wolfram, Phys. Rev. Lett. **29**, 1383 (1972).

[41]T. Wolfram and L. Sutcu, Phys. Rev. B **31**, 7680 (1985).

[42]T. Akahane, K. R. Hoffmann, T. Chiba, and S. Berko, Solid State Commun. **54**, 823 (1985).

[43]J. P. Doumerc, in *The Metal-Nonmetal Transition in Disordered Systems,* Proceedings of the 19th Scottish Universities Summer School in Physics, St. Andrew, 1978, edited by L. R. Friedman and D. P. Tunstall (Edinburgh University Press, Edinburgh, 1978), p. 313.

[44]J. P. Doumerc, J. Marcus, M. Pouchard, and P. Hagenmuller, Mater. Res. Bull. **14**, 201 (1979).

[45]K. Sturm, Adv. Phys. **31**, 1 (1982).

[46]G. Paasch, Phys. Status Solidi **38**, K123 (1970).

[47]K. Sturm, Z. Phys. **28**, 1 (1977).

[48]S. Ichimaru, Rev. Mod. Phys. **54**, 1017 (1982).

[49]H. Ehrenreich and M. H. Cohen, Phys. Rev. **115**, 786 (1959).

[50]S. L. Adler, Phys. Rev. **126**, 413 (1962); N. Wiser, *ibid.* **129**, 62 (1963).

[51]K. Sturm, Z. Phys. **29**, 27 (1978).

[52]M. S. Haque and K. L. Kliewer, Phys. Rev. Lett. **29**, 1461 (1972); Phys. Rev. B **7**, 2416 (1973).

[53]J. Fink, Adv. Electron. Electron Phys. **75**, 121 (1989).

[54]J. Daniels, C. v. Festenberg, H. Raether, and K. Zeppenfeld, in *Optical Constants of Solids by Electron Spectroscopy,* edited by G. Höhler, Springer Tracts in Modern Physics Vol. 54 (Springer, New York, 1970).

[55]H. Raether, in *Excitation of Plasmons and Interband Transitions by Electrons,* edited by G. Höhler, Springer Tracts in Modern Physics Vol. 88 (Springer, New York, 1980).

[56]P. Livins, T. Aton, and S. E. Schnatterly, Phys. Rev. B **38**, 5511 (1988).

[57]A. v. Felde, Ph.D. thesis, University of Karlsruhe, 1988.

[58]J. N. Chazalviel, M. Campagna, G. K. Wertheim, and H. R. Shanks, Phys. Rev. B **16**, 697 (1977).

[59]S. Sawada and G. C. Danielson, Phys. Rev. **113**, 1008 (1959).

[60]J. Feinleib, W. J. Scouler, and A. Ferretti, Phys. Rev. **165**, 765 (1968). The background dielectric constant ϵ_∞ was deter-

mined via Eq. (8) from the data given in Ref. 60: $m^*=0.86$, $\hbar\Omega_P=5.50$ eV, and $\hbar\omega_P=2.18$ eV.

[61]P. A. Cox, M. D. Hill, F. Peplinskii, and R. G. Egdell, Surf. Sci. **141**, 13 (1984).

[62]As pointed out by Owen *et al.* (Ref. 25), Table I of Ref. 24 contains a misprint. Their γ values (corresponding to our Γ) have to be multiplied by a factor of 10.

[63]L. Soriano, M. Abbate, J. Vogel, J. C. Fuggle, A. Fernández, A. R. González-Elipe, M. Sacchi, and J. M. Sanz, Surf. Sci. **290**, 427 (1993), and references therein.

[64]A. v. Felde, J. Fink, T. Büche, B. Scheerer, and N. Nücker, Europhys. Lett. **4**, 1037 (1987).

[65]A. v. Felde, J. Sprösser-Prou, and J. Fink, Phys. Rev. B **40**, 10 181 (1989).

[66]K. Sturm, Solid State Commun. **27**, 645 (1978).

[67]H. Möller and A. Otto, Phys. Rev. Lett. **45**, 2140 (1981).

[68]H. Möller and A. Otto, Phys. Rev. Lett. **46**, 1707 (1981).

[69]K. Sturm, Phys. Rev. Lett. **46**, 1706 (1981).

[70]A. A. Quong and A. G. Eguiluz, Phys. Rev. Lett. **70**, 3955 (1993).

[71]J. Sprösser-Prou, A. v. Felde, and J. Fink, Phys. Rev. B **40**, 5799 (1989).

[72]G. Kalman, K. Kempa, and M. Minella, Phys. Rev. B **43**, 14 238 (1991).

[73]M. Taut and K. Sturm, Solid State Commun. **82**, 295 (1992).

[74]E. Lipparini, S. Stringari, and K. Takayanagi, J. Phys. Condens. Matter **6**, 2025 (1994).

[75]F. Aryasetiawan and K. Karlsson, Phys. Rev. Lett. **73**, 1679 (1994).

[76]P. Vashishta and K. S. Singwi, Phys. Rev. B **6**, 875 (1972).

[77]B. Dabrowski, Phys. Rev. B **34**, 4989 (1986).

[78]K. J. Krane, J. Phys. F **8**, 2133 (1978).

[79]J. H. Weaver and D. W. Lynch, Phys. Rev. B **6**, 3620 (1972).

[80]N. Nücker, U. Eckern, J. Fink, and P. Müller, Phys. Rev. B **44**, 7155 (1991).